Evaluation of diffusion models in breast cancer

Rafal Panek, Marco Borri, Matthew Orton, Elizabeth O'Flynn, Veronica Morgan,
Sharon L. Giles, Nandita deSouza, Martin O. Leach, and Maria A. Schmidt[a)]
Cancer Research UK Cancer Imaging Centre, Division of Radiotherapy and Imaging, The Institute of Cancer Research and Royal Marsden Hospital, Sutton, Surrey SM2 5PT, United Kingdom

Purpose: The purpose of this study is to investigate whether the microvascular pseudodiffusion effects resulting with non-monoexponential behavior are present in breast cancer, taking into account tumor spatial heterogeneity. Additionally, methodological factors affecting the signal in low and high diffusion-sensitizing gradient ranges were explored in phantom studies.

Methods: The effect of eddy currents and accuracy of b-value determination using a multiple b-value diffusion-weighted MR imaging sequence were investigated in test objects. Diffusion model selection and noise were then investigated in volunteers ($n = 5$) and breast tumor patients ($n = 21$) using the Bayesian information criterion.

Results: 54.3% of lesion voxels were best fitted by a monoexponential, 26.2% by a stretched-exponential, and 19.5% by a biexponential intravoxel incoherent motion (IVIM) model. High correlation (0.92) was observed between diffusion coefficients calculated using mono- and stretched-exponential models and moderate (0.59) between monoexponential and IVIM (medians: $0.96/0.84/0.72 \times 10^{-3}$ mm^2/s, respectively). Distortion due to eddy currents depended on the direction of the diffusion gradient and displacement varied between 1 and 6 mm for high b-value images. Shift in the apparent diffusion coefficient due to intrinsic field gradients was compensated for by averaging diffusion data obtained from opposite directions.

Conclusions: Pseudodiffusion and intravoxel heterogeneity effects were not observed in approximately half of breast cancer and normal tissue voxels. This result indicates that stretched and IVIM models should be utilized in regional analysis rather than global tumor assessment. Cross terms between diffusion-sensitization gradients and other imaging or susceptibility-related gradients are relevant in clinical protocols, supporting the use of geometric averaging of diffusion-weighted images acquired with diffusion-sensitization gradients in opposite directions. © 2015 Author(s). All article content, except where otherwise noted, is licensed under a Creative Commons Attribution 3.0 Unported License. [http://dx.doi.org/10.1118/1.4927255]

1. INTRODUCTION

In diffusion-weighted MR imaging (DWI), the exponential decay of the signal as a function of the diffusion-sensitization coefficient b is employed to calculate an apparent diffusion coefficient (ADC) for each voxel imaged.[1–5] Highly proliferating malignant tumors result in cell density higher than normal parenchyma and therefore more restricted water diffusion. This leads to decreased values of ADC and can be used for tumor detection, as well as for monitoring and predicting tumor response.[4,5] The signal attenuation, however, is not only a result of the random microscopic motion of water molecules influenced by cell density, membrane integrity, and tissue microstructure but it also depends on microperfusion and diffusion heterogeneity within a voxel. As a result, signal behavior cannot always be reliably described by a simple monoexponential decay and more complex parametric models are increasingly used.[6–13] Effects associated with microcirculation in capillary networks and other transport mechanisms can affect the signals in low b-value images (<200 s/mm^2), as described in the intravoxel incoherent motion (IVIM) model.[8–13] Moreover,

in the presence of additional "nondiffusion" field gradients, such as imaging or susceptibility-related intrinsic gradients, signal attenuation depends on the square of the sum of gradients involved. This may lead to a miscalculation of the diffusion-sensitization coefficient b. In order to exclude such terms together with additional concomitant fields associated with the bipolar diffusion encoding, a geometric average of pairs of images acquired with opposite diffusion gradient directions and monopolar sequence can be used.[14–16] In addition, eddy currents[17] and lower SNR (Refs. 18 and 19) of high b-value images also compromise the quality of data fitting.

The purpose of this study was to investigate whether the microvascular pseudodiffusion effects resulting with non-monoexponential behavior significantly affect the diffusion-weighted signals in breast cancer taking into account tumor spatial heterogeneity. Additionally, methodological factors affecting the signal in low and high diffusion gradient ranges were explored in phantom studies. In particular, image distortion due to eddy currents, inaccuracy of b-value determination due to cross terms between diffusion-sensitizing and imaging gradients, and noise levels were considered.

2. METHODS

All imaging was performed on a 3 T MRI scanner (Philips Achieva, Best, Netherlands) using a dedicated seven-channel breast coil.

2.A. Multiple *b*-value DWI protocol

A diffusion-weighted protocol was implemented with ten *b*-values and diffusion-sensitization gradients applied in nine different directions. Pairs of diffusion-sensitization gradients parallel and antiparallel to imaging gradients directions and at 45° to the imaging gradients directions were applied. The range of *b*-values employed was from 0 to 1150 s/mm^2 (Table I). All diffusion-weighted images were coregistered to the $b = 0$ image prior to quantitative analysis using a rigid body 3D transformation available from the manufacturer's software. Data were analyzed offline using in-house developed MATLAB software (Mathworks, Cambridge MA).

2.A.1. System characterization

2.A.1.a. Eddy currents. Image distortion was evaluated using a structured test object (5 mm rods in a 200 mm diameter cylindrical phantom filled with a solution of 10 mM $CuSO_4$ in distilled water) by comparing the $b = 0$ reference images with diffusion-weighted images acquired sequentially for three orthogonal diffusion gradient directions (frequency, phase encoding, and slice imaging). Three angulations (0°, 15°, and 30°) with respect to the sagittal imaging plane were tested in order to investigate the influence of gradient system geometry on eddy currents. The centers of the phantom rods were used to map the distortion by measuring the distances between the $b = 0$ and diffusion-weighted images ($b = 50, 100, 200, 300, 400, 600, 800, 1000,$ and 1150).

2.A.1.b. Accuracy of ADC and linearity of diffusion signal attenuation. Temperature controlled measurements (21 °C) of uniform water and sucrose[20] phantoms (200 mm spheres containing distilled water with the addition of 10 mM $CuSO_4$ or 500 g/l sucrose, Sigma-Aldrich) were performed to assess signal attenuation and measured ADC values. A ROI encompassing 80% of both the water and sucrose spherical phantoms (central slice) was used to evaluate the calculated ADC values avoiding partial volume effects.[21] ADC values were first calculated separately for opposite directions of the diffusion-sensitizing gradients and compared with the geometrically averaged ADC value.

2.A.2. Clinical studies

Twenty-six women, including 21 with known breast cancer (median age 52, range: 37–81 yr) and 5 healthy volunteers (median age 30, range: 28–33 yr) underwent a breast MRI examination with approval from the Research Ethics Committee and with written informed consent. Patients with biopsy-proven breast cancer had only the tumor-containing breast scanned using the DWI protocol.

2.B. MR imaging protocol

A high resolution T_2-weighted TSE VISTA sequence (125 axial slices, 340 mm FOV, TE/TR = 220/2230 ms, and $1.2 \times 1.2 \times 3$ mm voxel reconstructed to $0.94 \times 0.94 \times 3$ mm) was acquired initially to plan DWI across the center of the lesion. Conventional DWI sequence with full breast coverage was performed first (sagittal SS-EPI, 180 mm FOV, 3 mm slice thickness, SPAIR and a slice-selection gradient reversal fat suppression, 4 *b*-values 0, 350, 750, 1150 mm^2/s, TR/TE = 3771/66 ms, and $1.96 \times 2.02 \times 3$ mm voxel) and followed by the multiple *b*-value DWI sequence described earlier (parameters summarized in Table I). Finally, T_1-weighted sequence (sagittal, 3D GRE, TR/TE = 4.5/2.3 ms, FA = 16°, 180 mm FOV, and $2.37 \times 2.4 \times 6$ mm acquisition voxel reconstructed to $0.94 \times 0.94 \times 3$ mm) with intravenous injection of 0.2 ml/kg of gadoterate meglumine was used to assist in the lesion identification and ROI positioning.

In the case of volunteer examinations, both breasts were scanned using T_2-weighted TSE VISTA (full breast coverage) and multiple *b*-value DWI sequences (three central slices).

2.C. Image processing and analysis

Regions of interest were drawn manually using postcontrast T_1-weighted and high *b*-value images [DWI sequence, $b = 1000$ s/mm^2, Fig. 1(B)] for tumor and on fat suppressed T_2-weighted $b = 0$ EPI images for normal parenchyma.

Regions with ADC $> 2 \times 10^{-3}$ mm^2/s and an absence of contrast uptake on T_1-weighted images (necrotic or cystic regions) were excluded from the ROIs.[22] Parametric maps

TABLE I. Diffusion-weighted MR imaging protocol parameters used in the study.

| Parameter	Value
MRI system	3 T (Philips Achieva, Best, Netherlands)
Pulse sequence	Single shot spin echo EPI
TE/TR (ms)	79/1000
Number of averages	3
FOV (mm)	180
Matrix	192×192
Slice thickness (mm)	3
Number of slices	3
Distance factor	0
Half-scan factor	0.68
SENSE	No
Orientation	Sagittal
Phase encode direction	Superior to inferior
Receiver bandwidth (Hz/pixel)	2310
b-values (s/mm^2)	0, 50, 100, 200, 300, 400, 600, 800, 1000, 1150
Total number and directions of diffusion-sensitizing gradients (image coordinate system was used with *M*—measurement, *P*—phase, and *S*—slice)	9 (-*P* / *S* / -*M* / *P* / -*S* / *M* / -*P* > Tra45/ *M* > Tra45/*M* > Cor45)
Fat suppression	SPAIR
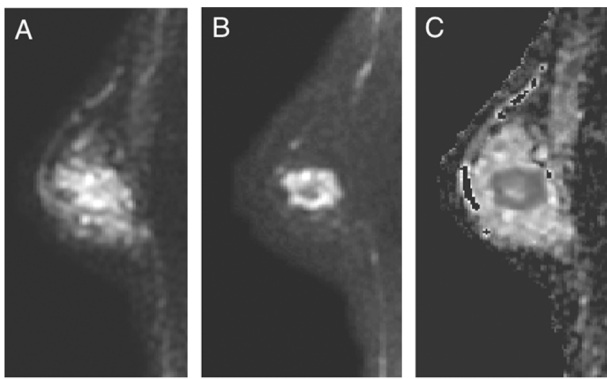
FIG. 1. Example of MRI diffusion images [(A) $b = 0$ s/mm^2, (B) $b = 1000$ s/mm^2, and (C) ADC map] of 51 yr-old patient with invasive ductal carcinoma in the right breast.

of ADC (Refs. 1–5) and SNR (Ref. 23) were calculated pixel by pixel for ROIs in the tumor and in healthy breast tissue (patients and volunteers) using MATLAB.

2.D. Diffusion signal modeling

In this study, three diffusion attenuation models were considered. The first model assumes a pure diffusion process and is described by a monoexponential decay of the measured signal S_1 as a function of b-value,

$$S_1(b) = S_0 e^{-b \cdot \text{ADC}}, \tag{1}$$

where S_0 is the initial signal acquired without diffusion weighting ($b = 0$) and ADC is the apparent diffusion coefficient. The

second model is described by a stretched-exponential function.[6,7]

$$S_2(b) = S_0 e^{-b \cdot \text{DDC}^\alpha} \tag{2}$$

in which DDC is the distributed diffusion coefficient and α is the heterogeneity index ranging from 0 to 1. In the case of homogeneous diffusion $\alpha = 1$, and the function simplifies to the monoexponential decay described by the first model. Lower values of α result either from nonexponential behavior caused by the addition of proton pools with a range of diffusion rates within the imaged voxel or from a process where the motion is intermittent.[7] The third model was the biexponential IVIM model, which accounts for a microcapillary perfusion and other flow effects contributing to signal attenuation at low b-values,

$$S_3(b) = S_0 \cdot (f e^{-b \cdot D^*} + (1-f) e^{-b \cdot D}). \tag{3}$$

This model is parameterized by the pseudodiffusion flow fraction f, the pseudodiffusion rate constant D^*, and the diffusion rate constant D.[8–11] Median ROI values were calculated for ADC, DDC, and D.

The penalized-likelihood Bayesian information criterion[24] (BIC) was used to assess how well each of the three models is supported by the data (MATLAB, Econometrics Toolbox),

$$\text{BIC} = -2\log L(\theta) + k \cdot \log(N), \tag{4}$$

where $L(\theta)$ is the value of the maximized likelihood objective function for a model with k parameters and N data points. Given any two estimated models, the model with the lower value of BIC is the one to be preferred. BIC differences
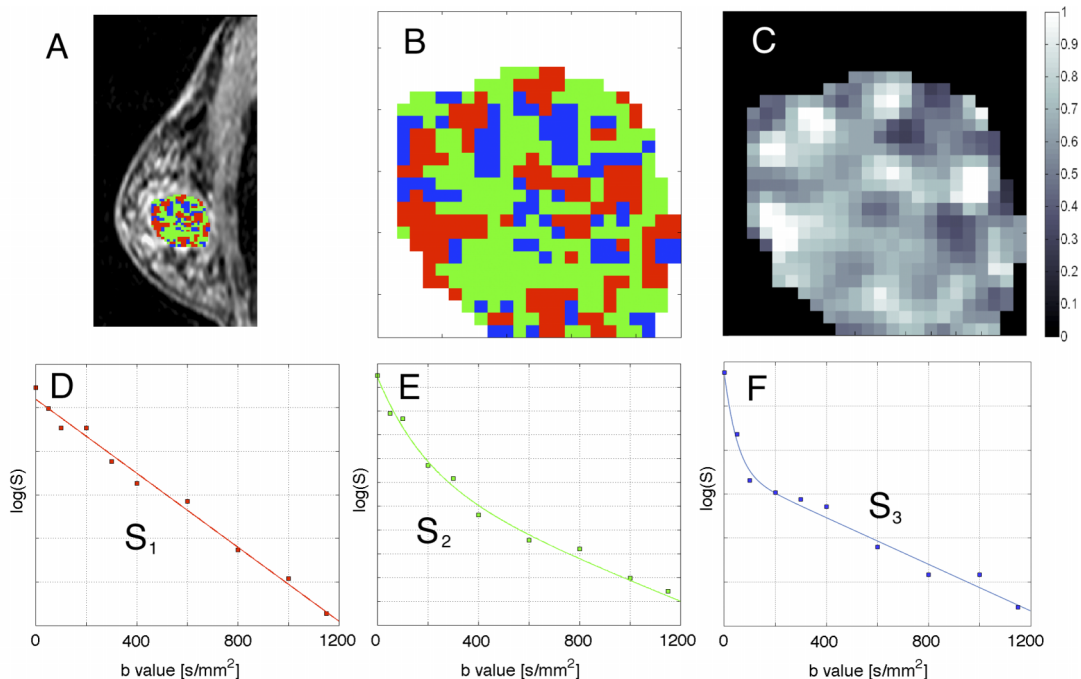

FIG. 2. (A) An example of lesion ROI overlaid on an anatomical T_2-weighted image. (B) Model selection map showing regions where monoexponential (S_1), stretched-exponential (S_2), and biexponential (S_3) models were best supported by the data (smallest Bayesian information criterion). (C) An alpha parameter map for the stretched-exponential model. A high alpha value close to unity shows a preference for the monoexponential model. (D)–(F) Examples of measured signal (log S) as a function of diffusion weighting (b-values) for voxels with different models selected using BIC [(D) monoexponential, (E) stretched-exponential, and (F) biexponential IVIM].

between the models are considered significant, strong, and very strong for $\Delta BIC = 2\text{–}6$, $6\text{–}10$, and >10, respectively.[25]

For each voxel, the model with the lowest BIC value was chosen and displayed in the form of model selection maps (Fig. 2) and used to calculate overall percentage model preferences. Correlation between measured ADC, DDC, and D was measured for all ROI voxels. Correlations between SNR and BIC values for each model were also used to assess if the signal to noise levels had an influence on model fitting.

2.E. Statistical analysis

The Wilcoxon signed-rank test[26] was used to compare malignant and healthy tissue diffusion parameters. Kendall's tau (τ)[27] was used to test for correlations. The null hypothesis was that there was no correlation between measured parameters. The strength of correlation was tested and the values were considered significant if $P < 0.05$. Statistical analysis was performed using the MATLAB Statistics Toolbox.

3. RESULTS

Four out of 26 subjects were excluded from the study because of fat suppression failure.

3.A. Image distortion

The eddy-current-related distortion, in the image phase encoding direction, was strongly dependent on the direction of the diffusion gradient (Table II) but not on the imaging plane angulation between 0° and 30°. The observed image stretch and displacement varied between 1 and 6 mm.

The sensitization gradient direction resulting in minimum image misregistration was along the phase-encode imaging gradient (sagittal: head–feet), corresponding to the z-axis of the scanner. The largest displacement observed for this direction in the b-value range between 1000 and 1150 s/mm^2 was 2 mm (see Table II). Only the data acquired with the diffusion-sensitization gradients along the phase encoding direction (superior–inferior) in the range of 0–800 s/mm^2 were used to model diffusion behavior in order to minimize the

TABLE II. The maximum image misregistration (mm) observed for different directions of the diffusion gradients in a sagittal breast DWI protocol. Frequency/phase/slice corresponds to $y/z/x$ scanner coordinates in the sagittal orientation.

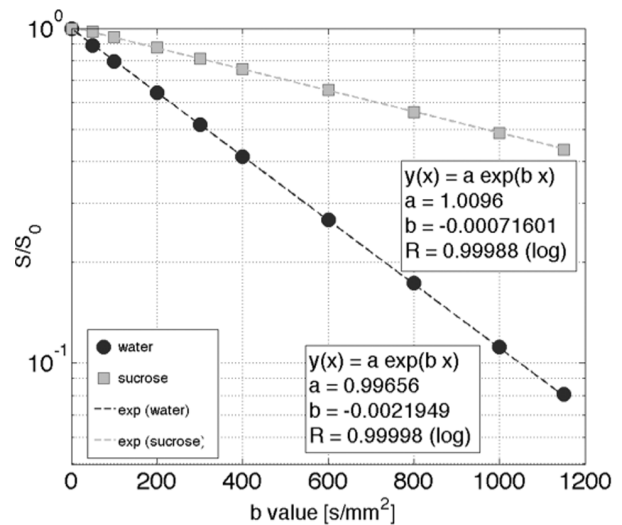| G_{diff}	Frequency	Phase	Slice
$b = 50$	1	0	0
$b = 100$	1	0	0
$b = 200$	1	0	0
$b = 300$	2	1	1
$b = 400$	2	1	1
$b = 600$	3	1	2
$b = 800$	3	1	2
$b = 1000$	4	2	3
$b = 1150$	6	2	3

FIG. 3. The b-value dependence on normalized DWI signal for water and sucrose (500 g/l) at 21 °C.

displacement of individual voxels with increasing b-values, as observed in the phantom work.

3.B. Accuracy and measured ADC values

The signal attenuation as a function of diffusion gradient b-value in phantoms is monoexponential (Fig. 3) and $BIC_{S_1} << BIC_{S_{2,3}}$.

ADC values measured with no geometric averaging depend on the direction of the diffusion gradient used [Fig. 4(A)].

With the diffusion gradient parallel and antiparallel to the phase encoding direction, the median ADC values were 2.17 and $2.2 \pm 0.02 \times 10^{-3}$ mm^2/s and 0.72 and $0.75 \pm 0.03 \times 10^{-3}$ mm^2/s for the water and sucrose phantoms, respectively. ADC values measured using geometrically averaged pairs of images (opposite diffusion gradient directions) differed statistically from nonaveraged values ($p < 0.05$) and these values were $2.18 \pm 0.02 \times 10^{-3}$ mm^2/s and $0.74 \pm 0.02 \times 10^{-3}$ mm^2/s for water and sucrose, respectively [Fig. 4(B)].

Figure 1 shows a clinical example of low [Fig. 1(A)] and high [Fig. 1(B)] b-value DWI-EPI images (multiple
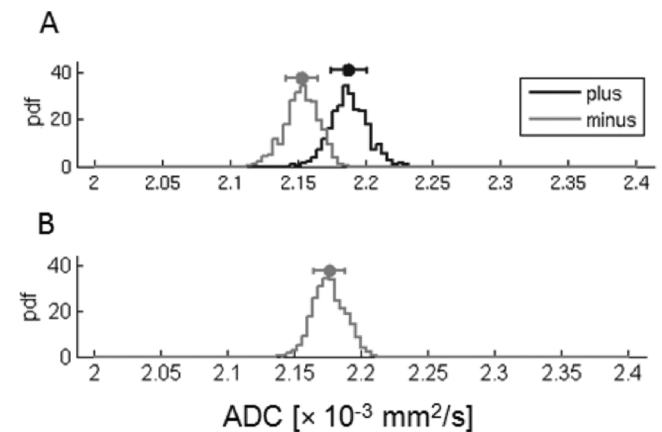

FIG. 4. Histograms of ADC values for diffusion-sensitization gradient in two opposite directions (plus and minus) measured for water (21 °C) (A) and a histogram for geometrically averaged data (B).
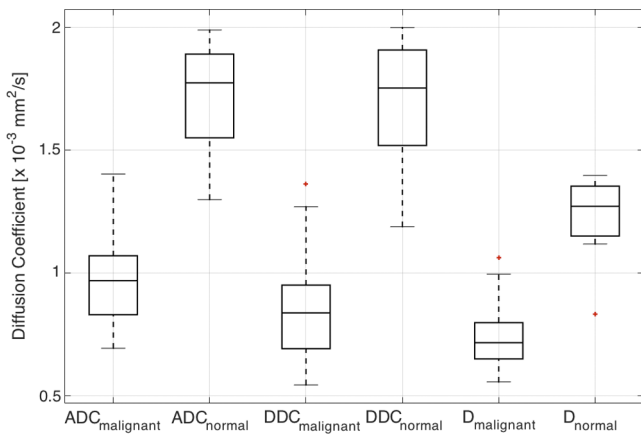
FIG. 5. A comparison of patient median ADC, DDC, and *D* in malignant and normal breast tissue. All diffusion coefficients were significantly higher in the normal tissue than in malignant lesions ($P_{S_{1-3}} < 0.001$).

b-value sequence). ADC values [Fig. 1(C)] obtained from ROIs in normal breast tissue were significantly higher than in malignant lesions ($P < 0.001$). The median ADC value for the parenchyma was 1.76×10^{-3} and 0.96×10^{-3} mm^2/s for breast cancer (Fig. 5).

3.C. Noise

The SNR distribution calculated for breast ROIs at the *b*-value 800 s/mm^2 was positively skewed with median values of 10.09 in tumor and 2.18 in the normal breast tissue. There was no correlation between SNR and the BIC values calculated for the models used (tumor: $\tau_{S_1} = 0.05$, $\tau_{S_2} = -0.03$, $\tau_{S_3} = 0.07$ and parenchyma: $\tau_{S_1} = 0.03$, $\tau_{S_2} = 0.08$, $\tau_{S_3} = 0.11$).

3.D. Model selection

A high correlation was observed between diffusion coefficients calculated using mono- and stretched-exponential models ($\tau_{tumor} = 0.92$, $\tau_{parenchyma} = 0.9$). A moderate correlation was found between the monoexponential model and IVIM ($\tau_{tumor} = 0.59$, $\tau_{parenchyma} = 0.53$). Median values were 0.96, 0.84, and 0.72×10^{-3} mm^2/s for ADC (S_1), DDC (S_2), and *D* (S_3), respectively, in tumor and 1.76, 1.75, and 1.24 $\times 10^{-3}$ mm^2/s in normal breast parenchyma (Fig. 5). All diffusion coefficients were significantly higher in the normal tissue than in malignant lesions ($P_{S_{1-3}} < 0.001$). The Bayesian information criteria from the lesion ROI data showed that 54.3% of voxels were best fitted by the monoexponential, 26.2% by the stretched-exponential, and 19.5% by the biexponential IVIM model ($N_{voxels} = 4601$). In 83% of voxels, the BIC difference between the models was considered significant[25] with 66% positive, 9% strong, and 8% very strong evidence. Figure 2 shows an example of a model selection map and the corresponding alpha parameter map. The distribution of the stretched-exponential alpha parameter in the tumor is negatively skewed ($\gamma_1 = -0.9$) with a median value of $\alpha_{tumor} = 0.75$, the pseudodiffusion rate constant $D^*_{tumor} = 21.5 \times 10^{-3}$ mm^2/s, and the pseudodiffusion flow fraction $f_{tumor} = 0.15$.

In the normal parenchyma, 58.3% of voxels were best fitted by the monoexponential, 24.6% by the stretched-exponential, and 17.1% by the biexponential IVIM model ($N_{voxels} = 5022$). In 83% of voxels, the BIC difference between the models was considered significant with 68% positive, 8% strong, and 7% very strong evidence. The distribution of the stretched-exponential alpha parameter in the parenchyma is negatively skewed ($\gamma_1 = -0.92$) with a median value of $\alpha_{parenchyma} = 0.8$, the pseudodiffusion rate constant $D^*_{parenchyma} = 16.8 \times 10^{-3}$ mm^2/s, and the pseudodiffusion flow fraction $f_{parenchyma} = 0.08$.

4. DISCUSSION

Diffusion-weighted imaging is increasingly being used for cancer detection and diagnosis. However, it is still an open question as to which models are appropriate for DWI in various body regions and cancer types characterized by different microscopic environments.

Initial implementations of IVIM in the breast have been reported indicating the feasibility of perfusion fraction and pseudodiffusion coefficient measurements[13] in addition to the diffusion coefficient. A biexponential characterization of the diffusion attenuation signal has been reported for lesions, in contrast to a monoexponential dependence in normal tissue. These measurements were performed using the mean signal over ROIs and therefore disregard lesion heterogeneity, which is clearly observed in practice (Fig. 1). It has also been shown that the diffusion attenuation is no longer monoexponential at large *b*-values ($b > 2000$ s/mm^2)[28–32] including breast cancer preclinical studies,[33–35] and this effect is associated with restricted intracellular water diffusion rather than the properties of restricting boundaries in the extracellular space. Another confounding factor is fat signal, which depends on the choice of fat suppression technique, especially relevant in the case of higher *b*-value (>600 s/mm^2) breast DWI images.[36] Although clinical systems are increasingly capable of delivering higher *b*-values, it is likely that noise will dominate breast images acquired with clinical parameters and $b > 2000$ s/mm^2. Another concern is an assumption of the IVIM model, which states that time after diffusing particles change their direction is several times shorter than the total duration of diffusion gradients (i.e., 7 times–Le Bihan[9]). A recent study shows that this assumption is not met in liver and pancreas,[16] suggesting that a further development is needed to appropriately calculate pseudodiffusion coefficient D^*. There is, however, lack of evidence for similar shortcomings in breast parenchyma and lesions.

One of the methodological DWI caveats which is also a potential limitation of this work is a choice of *b*-values, which affects calculated diffusion coefficient values. The range of *b*-values used should be adjusted for expected diffusion values in the examined tissues, observed SNR levels, and eddy currents. *b*-values in the range of 0–800 s/mm^2 are commonly used in the breast and IVIM applications.[11–13]

In our work, the diffusion signal was analyzed for each pixel of ROIs defined in test objects, lesions, and normal

tissue. Test object images acquired with diffusion-sensitization gradients of opposite polarity produced significantly different ADC values, suggesting that other gradients contribute toward diffusion weighting. This highlights an essential issue in modeling diffusion behavior: cross terms between diffusion-sensitization gradients and other gradients were shown to be relevant (Fig. 4) and may induce error. In this work, geometrical averaging of images produced with diffusion-sensitization gradients of opposite polarity was used to minimize the effect of other gradients in order not to compromise the accuracy of the modeling. In addition, phantom work showed that geometrical distortion of high *b*-value images is significant (Table II) and can introduce errors in the ADC evaluation. In this work, only the data acquired with the diffusion-sensitization gradients along the phase encoding direction (superior–inferior) in the 0–800 s/mm^2 *b*-value range were used to model diffusion behavior, minimizing the error. Other practical solutions to reduce eddy current distortion are to use the bipolar diffusion gradient scheme;[15] however, the use of temporally asymmetric diffusion gradients leads to the presence of significant concomitant fields and undesired signal voids.[15,16]

Statistical model selection analysis suggests that the monoexponential model describes majority of the data most accurately. There was, however, evidence of regions with signal best described by stretched-exponential and IVIM models in both tumor and normal breast tissue. This might suggest a presence of increased structural heterogeneity or microperfusion and might be of clinical use. The parameter alpha may be used to identify regions showing significantly non-monoexponential behavior [lower alpha, Figs. 2(B) and 2(C)]. Median diffusion coefficients calculated using all three models show significant differences between tumor and normal breast parenchyma. Data distribution representing intratumoral heterogeneity (Fig. 5) reveals greater overlap between malignant and normal tissues in the case of IVIM model. The median IVIM diffusion coefficients are markedly lower than the analogous parameters from other models. This could be a consequence of a signal fit bias for smaller *b*-values in the presence of pseudodiffusion and as a result higher DDC and ADC values.[37]

An important feature of the Bayesian information criterion is that more complex models are appropriately penalized relative to simpler models that fit the data equally well, given the data SNR.[24] Correlations are not observed between the SNR and the penalized-likelihood BIC for the models considered. This indicates the preference for stretched-exponential model is unrelated to noise levels. In the case of insufficient SNR, a pure diffusion process characterized correctly by a monoexponential decay would appear artificially stretched in the higher *b*-value region due to a noise-floor effect, which would lead to a correlation between SNR and BIC values.

5. CONCLUSIONS

Cross terms between diffusion-sensitization gradients and other gradients (either imaging gradients or susceptibility-related gradients) are relevant in clinical protocols, supporting the use of geometric averaging of diffusion-weighted images acquired with diffusion-sensitization gradients in opposite directions. Microcirculatory pseudodiffusion and intravoxel heterogeneity effects were not observed in approximately half of normal and malignant breast tissue. This result indicates that stretched and IVIM models should be utilized in local voxel analysis rather than global tumor assessment.

a)Author to whom correspondence should be addressed. Electronic mail: Maria.Schmidt@icr.ac.uk; Telephone: +44 (0)20 8661 3353; Fax: +44 (0)20 8915 6718.

[1]E. O. Stejskal and J. E. Tanner, "Spin diffusion measurements: Spin echoes in the presence of a time-dependant field gradient," J. Chem. Phys. **42**, 288–292 (1965).

[2]J. E. Tanner and E. O. Stejskal, "Restricted self-diffusion of protons in colloidal systems by the pulsed-gradient, spin-echo method," J. Chem. Phys. **49**, 1768–1777 (1968).

[3]D. Le Bihan, "Molecular diffusion nuclear magnetic resonance imaging," Magn. Reson. Q. **7**, 1–30 (1991).

[4]L. Gray and J. MacFall, "Overview of diffusion imaging," Magn. Reson. Imaging Clin. North Am. **6**, 125–138 (1998).

[5]H. A. Rowley, P. E. Grant, and T. P. L. Roberts, "Diffusion MR imaging. Theory and applications," Neuroimaging Clin. North Am. **9**, 343–361 (1999).

[6]K. M. Bennett, K. M. Schmainda, R. T. Bennett, D. B. Rowe, H. Lu, and J. S. Hyde, "Characterization of continuously distributed cortical water diffusion rates with a stretched-exponential model," Magn. Reson. Med. **50**, 727–734 (2003).

[7]Y. Mazaheri, A. Afaq, D. B. Rowe, Y. Lu, A. Shukla-Dave, and J. Grover, "Diffusion-weighted magnetic resonance imaging of the prostate: Improved robustness with stretched exponential modeling," J. Comput. Assisted Tomogr. **36**, 695–703 (2012).

[8]D. Le Bihan, E. Breton, D. Lallemand, P. Grenier, E. Cabanis, and M. Laval-Jeantet, "MR imaging of intra-voxel incoherent motions: Application to diffusion and perfusion in neurologic disorders," Radiology **161**, 401–407 (1986).

[9]D. Le Bihan, E. Breton, D. Lallemand, M. L. Aubin, J. Vignaud, and M. Laval-Jeantet, "Separation of diffusion and perfusion in intravoxel incoherent motion MR imaging," Radiology **168**, 497–505 (1988).

[10]D. Le Bihan, R. Turner, C. T. Moonen, and J. Pekar, "Imaging of diffusion and microcirculation with gradient sensitization: Design, strategy, and significance," J. Magn. Reson. Imaging **1**, 7–28 (1991).

[11]D. Le Bihan, "IVIM method measures diffusion and perfusion," Diagn. Imaging **12**, 133–136 (1990).

[12]D. M. Koh, D. J. Collins, and M. R. Orton, "Intravoxel incoherent motion in body diffusion-weighted MRI: Reality and challenges," Am. J. Roentgenol. **196**, 1351–1361 (2011).

[13]E. E. Sigmund, G. Y. Cho, S. Kim, M. Finn, M. Moccaldi, J. H. Jensen, D. K. Sodickson, J. D. Goldberg, S. Formenti, and L. Moy, "Intravoxel incoherent motion imaging of tumor microenvironment in locally advanced breast cancer," Magn. Reson. Med. **65**, 1437–1447 (2011).

[14]R. F. Karlicek, Jr. and I. J. Lowe, "A modified pulsed gradient technique for measuring diffusion in the presence of large background gradients," J. Magn. Reson. **37**, 75–91 (1980).

[15]M. A. Bernstein, X. J. Zhou, J. A. Polzin, K. F. King, A. Ganin, N. J. Pelc, and G. H. Glover, "Concomitant gradient terms in phase contrast MR: Analysis and correction," Magn. Reson. Med. **39**, 300–308 (1998).

[16]A. Wetscherek, B. Stieltjes, and B. F. Laun, "Flow-compensated intravoxel incoherent motion diffusion imaging," Magn. Reson. Med. (in press) (2014).

[17]G. K. Rohde, A. S. Barnett, P. J. Basser, S. Marenco, and C. Pierpaoli, "Comprehensive approach for correction of motion and distortion in diffusion-weighted MRI," Magn. Reson. Med. **51**, 103–114 (2004).

[18]R. M. Henkelman, "Measurement of signal intensities in the presence of noise in MR images," Med. Phys. **12**, 232–233 (1985).

[19]N. G. Papadakis, K. M. Martin, I. D. Wilkinson, and C. L. Huang, "A measure of curve fitting error for noise filtering diffusion tensor MRI data," J. Magn. Reson. **164**, 1–9 (2003).

[20]National Electrical Manufacturers Association, Determination of Image Uniformity in Diagnostic Magnetic Resonance Images, Document No. MS3, 1989.

[21]S. H. Park, K. H. Chang, I. C. Song, Y. J. Kim, S. H. Kim, and M. H. Han, "Diffusion-weighted MRI in cystic or necrotic intracranial lesions," Neuroradiology **42**, 716–721 (2000).

[22]I. Delakis, E. M. Moore, M. O. Leach, and J. P. De Wilde, "Developing a quality control protocol for diffusion imaging on a clinical MRI system," Phys. Med. Biol. **49**, 1409–1422 (2004).

[23]R. R. Price, L. Axel, and T. Morgan, "Quality assurance methods and phantoms for magnetic resonance imaging: Report of AAPM nuclear magnetic resonance Task Group No 1a," Med. Phys. **17**, 287–295 (1990).

[24]G. E. Schwarz, "Estimating the dimension of a model," Ann. Stat. **6**, 461–464 (1978).

[25]R. E. Kass and A. E. Raftery, "Bayes factors," J. Am. Stat. Assoc. **90**, 773–795 (1995).

[26]F. Wilcoxon, "Individual comparisons by ranking methods," Biom. Bull. **1**(6), 80–83 (1948).

[27]M. Kendall, "A new measure of rank correlation," Biometrika **30**, 81–89 (1938).

[28]J. H. Jensen, J. A. Helpern, A. Ramani, H. Lu, and K. Kaczynski, "Diffusional kurtosis imaging: The quantification of non-gaussian water diffusion by means of magnetic resonance imaging," Magn. Reson. Med. **53**, 1432–1440 (2005).

[29]H. Lu, J. H. Jensen, A. Ramani, and J. A. Helpern, "Three-dimensional characterization of non-gaussian water diffusion in humans using diffusion kurtosis imaging," NMR Biomed. **19**, 236–247 (2006).

[30]P. Raab, E. Hattingen, K. Franz, F. E. Zanella, and H. Lanfermann, "Cerebral gliomas: Diffusional kurtosis imaging analysis of microstructural differences," Radiology **254**, 867–875 (2010).

[31]J. J. Wang, W. Y. Lin, C. S. Lu, Y. H. Weng, S. H. Ng, C. H. Wang, H. L. Liu, R. H. Hsieh, Y. L. Wan, and Y. Y. Wai, "Parkinson disease: Diagnostic utility of diffusion kurtosis imaging," Radiology **261**, 210–217 (2011).

[32]J. Zhuo, S. Xu, J. L. Proctor, R. J. Mullins, J. Z. Simon, G. Fiskum, and R. P. Gullapalli, "Diffusion kurtosis as an *in vivo* imaging marker for reactive astrogliosis in traumatic brain injury," NeuroImage **59**, 467–477 (2012).

[33]C. F. Maier, Y. Paran, P. Bendel, B. K. Rutt, and H. Degani, "Quantitative diffusion imaging in implanted human breast tumors," Magn. Reson. Med. **37**, 576–581 (1997).

[34]J. Pfeuffer, S. W. Provencher, and R. Gruetter, "Water diffusion in rat brain *in vivo* as detected at very large b values is multicompartmental," Magn. Reson. Mater. Biol., Phys., Med. **8**, 98–108 (1999).

[35]Y. Cohen and Y. Assaf, "High b-value q-space analyzed diffusion-weighted MRS and MRI in neuronal tissues—A technical review," NMR Biomed. **15**, 516–542 (2002).

[36]P. Baron, M. D. Dorrius, P. Kappert, M. Oudkerk, and P. E. Sijens, "Diffusion-weighted imaging of normal fibroglandular breast tissue: Influence of microperfusion and fat suppression technique on the apparent diffusion coefficient," NMR Biomed. **23**, 399–405 (2010).

[37]S. Walker-Samuel, M. Orton, L. D. McPhail, and S. P. Robinson, "Robust estimation of the apparent diffusion coefficient (ADC) in heterogeneous solid tumors," Magn. Reson. Med. **62**, 420–429 (2009).